Dynamics of Amorphous and Semicrystalline 1,4-*trans*-Poly(isoprene) by Dielectric Spectroscopy

Silvina Cerveny,*,† Philippe Zinck,‖ Michael Terrier,‖ Silvia Arrese-Igor,† Angel Alegría,†,‡ and Juan Colmenero†,‡,§

Centro de Física de Materiales, Centro Mixto CSIC-UPV/EHU, Paseo Manuel de Lardizabal 4, 20018, San Sebastián, Spain, Departamento de Física de Materiales, Facultad de Química, Universidad del País Vasco (UPV/EHU), Apartado 1072, 20018, San Sebastián, Spain, Donostia Internacional Physics Center, Paseo Manuel de Lardizabal 4, 20018, San Sebastián, Spain, and Synthèses Organométalliques et Catalyse, Unité de Catalyse et Chimie du Solide, UMR CNRS 8181, USTL-ENSCL, Cité Scientifique, 59652 Villeneuve d'Ascq, France

Received July 22, 2008; Revised Manuscript Received September 15, 2008

ABSTRACT: We have studied the dynamics of amorphous 1,4-trans-poly(isoprene) (*trans*-PI) with different molecular weights using broadband dielectric spectroscopy over a wide range of temperature $\sim T_g - 70$ K to $T_g + 130$ K, and frequencies (10^{-1} to 10^6 Hz). Avoiding crystallization by quenching, three dielectric processes (global chain, segmental and local relaxations) were observed in order of decreasing temperature. Both the segmental and local relaxations of the here studied *trans*-PI, were found to be markedly different compared with the corresponding processes in *cis*-PI. In contrast, the temperature dependence of the relaxation time related to the global chain mode was found to be independent of the chain configuration. However, its relaxation strength was 1 order of magnitude lower in *trans*- than in *cis* configuration indicating a small parallel component of the dipole moment in *trans* configuration. In addition we also studied the dielectric spectra of *trans*-PI upon crystallization. The kinetics during crystallization as observed by dielectric spectroscopy results independent of molecular weight. During isothermal crystallization the dielectric spectra can be analyzed by a combination of three processes: the α_m-relaxation related with the modified amorphous phase, the so-called α_{CAP}-relaxation induced by crystallization and the β-relaxation, the two later only varying in relaxation strength. At the end of isothermal crystallization a percentage of crystallinity about 30% was estimated.

Introduction

The dynamics of 1,4-*cis*-poly(isoprene) (*cis*-PI) by using dielectric spectroscopy were studied originally by Adachi and Kotaka[1−3] over 20 years ago. They showed that, in addition to the segmental process, there was a molecular-weight-dependent process corresponding to long-range motions. Since these studies PI has been the subject of extensive experimental investigation by using different techniques such as dielectric and mechanical spectroscopy, nuclear magnetic resonance (NMR), neutron scattering and molecular dynamics simulations.[4−13] It has also been deeply studied as a component in block copolymers or in polymeric blends.[10,14−17] As PI can be synthesized with different microstructures (1,4-*cis*, 1,4-*trans*, and 3,4 configurations) and molecular weights, it has a wide range of applications from tire to textile industries. The *cis* isomer, predominant in natural rubber (NR), is produced by several plants being an industrial important polymer whereas the *trans* isomer (gutta percha) is synthesized by much fewer plants, but nevertheless used for many applications and included in several formulations of industrial materials due to its resistance of biological degradation.[18] However, most of the experimental and theoretical effort was focused on *cis*-PI. To our knowledge, there are not yet extensive experimental measurements on the *trans* conformer. In the last years, there have been some activity in the field of molecular dynamic simulations at about room temperatures[19,20] but its dynamical behavior in a broad temperature range was not yet reported in the literature.

On the other hand, PI has net electrical dipole component parallel to the chain contour (the so-called type A dipole in the Stockmayer classification[21]). Therefore it exhibits, in addition to the segmental relaxation (or α-relaxation) and local relaxation (or β-relaxation), a global chain relaxation process (or normal mode relaxation). The segmental relaxation is due to fluctuations of the dipoles perpendicular to the chain backbone whereas the dielectric normal mode relaxation reflects the fluctuations of the end-to-end vector. As above-mentioned, Adachi and coworkers[1−3] published a series of papers describing dielectric measurements on both the segmental and terminal modes of linear *cis*-PI with different molecular weights. More recently, Watanabe et al.[22,23] have also reported several works by both mechanical and dielectric spectroscopy in *cis*-PI having different architectures. From these works, it is well-known that the local and segmental relaxations of *cis*-PI have relaxation times independent of the chain molecular weight whereas the normal mode relaxation time (τ_{NM}) strongly depends on molecular weight.[22,23] However, there is no information in the literature about the dependence of the observed relaxations with the different configurations.

1,4-*trans*-Poly(Isoprene) (*trans*-PI) has the ability to crystallize in two different crystalline forms (α-form (monoclinic) and β-form (orthorhombic)) depending on the crystallization condition (crystallization temperature and molecular weight).[24−26] These studies have shown that the morphology obtained by direct crystallization is very complex with the observation of single lamellas and the multilamellar bodies. However, up to our knowledge there are not studies during cold crystallization (temperatures close to 220 K). Moreover, although its thermodynamic properties[27] and crystallinity[28] were studied in the literature, the dielectric spectra of amorphous *trans*-PI have not been reported in the literature. Subsequently, the evolution of the dielectric spectra from the amorphous phase to the semi-

* Corresponding author. E-mail: scerveny@ehu.es.
† Centro de Física de Materiales, Centro Mixto CSIC-UPV/EHU.
‡ Departamento de Física de Materiales, Facultad de Química, Universidad del País Vasco (UPV/EHU).
§ Donostia Internacional Physics Center.
‖ Synthèses Organométalliques et Catalyse, Unité de Catalyse et Chimie du Solide, UMR CNRS 8181, USTL-ENSCL.

10.1021/ma8016585 CCC: $40.75
Published on Web 10/23/2008

Table 1. Microstructure of the Samples Used in This Work[a]

sample	M_n [kg/mol]	M_w [kg/mol]	I_p	T_g (DSC) [K]
trans-PI-22K	22.8	27.4	1.20	201.1
trans-PI-33K	33.0	45.5	1.38	201.2
trans-PI-41K	41.2	51.9	1.26	201.3
trans-PI-49K	49.5	69.3	1.40	201.3
cis-PI	22.0	22.2	1.01	209.9

[a] M_n is the average molecular weight, M_w is the weight averaged molecular weight, T_g represents the glass transition temperature measured by DSC, and I_p is the polydispersivity index.

crystalline phase has not been analyzed so far. This particular aspect have been studied for many years in other polymers although there are some aspects that still remain controversial.[29−31]

The aim of this paper is to study the dynamics of *trans*-PI in both the amorphous and partially crystalline phases. At first, we report results from dielectric spectroscopy on amorphous *trans*-PI having different molecular weights. We provide information about the evolution of the dynamics between 150 K and 222 K (prior to cold crystallization) and also at higher temperatures from 290 K to 350 K. In addition, we show that both local and segmental dynamics of PI are highly dependent on configuration. After that, the isothermal evolution of the dielectric spectra from the amorphous to semicrystalline *trans*-PI is analyzed. We also discuss on the dynamics of the so-called constrained amorphous phase (CAP) obtained after crystallization.

Experimental Section

Materials. *trans*-Poly(Isoprene) was synthesized through transition metal catalysis. Further details concerning the synthesis can be found elsewhere.[32−34] After polymerization, the poly(isoprene) backbone is constituted mainly by *trans* units (97−98%). The molecular weight (M_n) and polydispersity index (determined from SEC experiments) of the samples investigated are listed in table 1. To avoid oxidation, PI samples were stored in light-protected flasks at −5 °C. In addition, since the dipolar moment of PI is small and the samples could contain a certain level of impurities, the samples for the dielectric experiment were further precipitated in excess methanol and then dried in a vacuum oven at 40 °C for 48 h.

Differential Scanning Calorimetry (DSC). The glass transition temperature (T_g) of all the compounds was determined by DSC (Q2000 TA Instrument). It is well-know that *trans*-PI can crystallize on cooling. To avoid crystallization during cooling, *trans*-PI was cooled at a rate of 50K/min and subsequently heated at rate of 10 K/min. The glass transition temperature was determined as the onset of the heat flow step of the heating trace.

Dielectric Spectroscopy. A broadband dielectric spectrometer, Novocontrol Alpha analyzer, was used to measure the complex dielectric function, $\varepsilon^*(\omega) = \varepsilon'(\omega) - i\,\varepsilon''(\omega)$, $\omega = 2\pi f$, in the frequency (f) range 10^{-1}−10^6 Hz. The samples were placed between parallel gold-plated electrodes with a diameter of 20 mm and they were directly quenched in liquid nitrogen to avoid crystallization upon cooling. Isothermal measurements were performed every 5 degree over the temperature range 140−200 K and every 2 deg over the temperature range 203−221 K. Finally, after melting the crystallized sample in the dielectric cryostat, isothermal measurements on the amorphous *trans*-PI in the high temperature range 355−290 K were performed every 5 deg. The temperature stability was in all the cases better than ±0.1 K. Note that a rather broad temperature range (221−290 K) is inaccessible for the dielectric experiment on the fully amorphous *trans*-PI.

The imaginary part of the obtained dielectric permitivitty was analyzed by the phenomenological Havriliak−Negami (HN) function[35]

$$\varepsilon^*(\omega) = \varepsilon_\infty + \frac{\Delta\varepsilon}{[1 + (i\omega\tau_{HN})^\alpha]^\gamma} \quad (1)$$

where $\Delta\varepsilon = \varepsilon_s - \varepsilon_\infty$, ε_∞ and ε_s are the unrelaxed and relaxed values of the dielectric constant and τ_{HN} is a characteristic relaxation time.

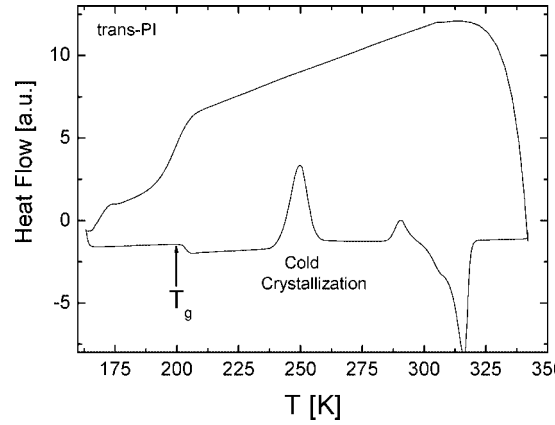

Figure 1. Differential scanning calorimetry (DSC) curve of *trans*-PI as a function of the temperature. Cooling curve shows as crystallization can be avoided at this fast cooling rate (50 K/min) whereas heating curve shows a clear glass transition at around 201.1 K followed by a cold crystallization at around 237 K.

In eq 1, α and γ are shape parameters ($0 < \alpha$, $\alpha\gamma \leq 1$) which describe the symmetric and the asymmetric broadening of the equivalent relaxation time distribution function. By setting $\alpha = \gamma = 1$ in eq 1, a Debye relaxation function is obtained; with $\gamma = 1$ a symmetrical function is obtained (Cole−Cole (CC) function[36]), which is widely used to describe secondary relaxations in glassy materials. An asymmetric Cole−Davidson function (CD) is obtained with $\alpha = 1$.[37]

Results

A. Calorimetric Results. A typical DSC scan showing the heat flow of pure *trans*-PI during cooling (rate = 50K/min) and heating (rate = 10K/min) is given in Figure 1. It is apparent that at this high cooling rate, it is possible to avoid crystallization on cooling obtaining a glass phase at low temperatures. Heating scan in figure 1 shows a glass transition followed by a cold crystallization at about 237K. After that, a broad melting transition with multiple peaks is observed in the temperature range between 285 and 320K. The T_g of all the samples were determined as the onset of the heat flow step and the resulting values are shown in Table 1. It is apparent that T_g values for *trans*-PI are independent of molecular weight in the range investigated, but significant lower than that of *cis*-PI.

B. Dielectric Relaxation on Fully Amorphous *trans*-Poly(isoprene). The frequency dependence of the dielectric loss permittivity, ε'', of *trans*-PI is shown in Figure 2 at some representative temperatures. In the vicinity of the glass transition temperature, the segmental relaxation (or α-relaxation) in the low frequency range is observed followed by a secondary process (β-relaxation) in the high-frequency range (see curve at $T = 205$ K). At much higher temperatures (see curves at 315 and 330 K), a new weak relaxation appears at lower frequencies somehow overlapped with the conductivity contribution. We have already mentioned in the introduction, that the PI chains have a dipolar component oriented parallel to the chain backbone and therefore the global chain motions are dielectrically active. As it will be confirmed below, this new relaxation corresponds in fact to the normal mode of *trans*-PI.

At temperatures below 220 K, the imaginary part of the dielectric spectrum of all samples was fitted by using one HN equation for the segmental relaxation whereas the secondary relaxation was described by a CC function. At higher temperatures only the normal mode is seen in the frequency window and, in this case, the dielectric response was described by using a CD function plus a power law to take into account the conductivity effects which dominate at low frequencies. As we

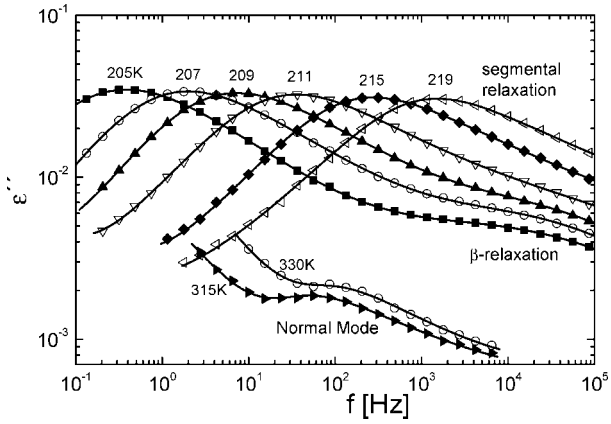

Figure 2. Loss component, ε'', of the complex dielectric permittivity, $\varepsilon^*(f)$, of *trans*-PI ($M_n = 41.2$ kg/mol) after quenching in liquid nitrogen. Three different relaxations can be observed: the segmental relaxation (α-relaxation), the local relaxation (β-relaxation) and the normal mode. Solid lines represent a least-squares fits as explained in the text.

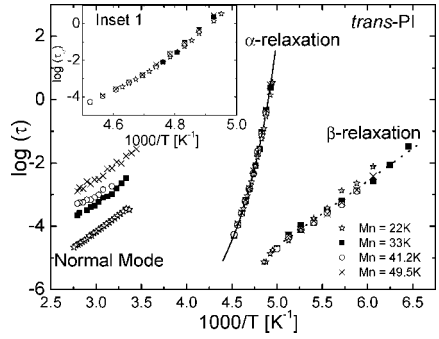

Figure 3. Plot of the characteristic relaxation times of *trans*-PI at different molecular weights. The solid lines thought the data points are fits of the VFT equation while the dotted lines display fits to the Arrhenius equation. Inset: Temperature dependence of the relaxation times corresponding to α-relaxation in a restricted scale to show its invariance with molecular weight.

mentioned above, in order to compare the dielectric response of *cis*- and *trans*-PI we have also measured a sample of *cis*-PI with a molecular weight $M_n = 22.2$ kg/mol. The fitting procedure applied to this sample was the following. For the α- and β- relaxations we have used a HN and a CC function respectively. In the case of the normal mode of *cis*-PI any single HN function is a good description of the data,[22] instead we have used the sum of a Debye and a CC function.

Apart from the fitting procedure, we have defined a characteristic time for the different processes as $\tau_{max} = 1/(2\pi f_{max})$ where f_{max} is the frequency of the corresponding maximum of ε''. In this way, the relaxation time results to be independent of any fitting frame. Figure 3 shows the so obtained relaxation times for *trans*-PI (full symbols) at different molecular weights. The inset 1 of Figure 3 shows the relaxation times corresponding to α-relaxation in more convenient scale. Figure 4 (parts a and b) shows both the α-relaxation and the normal mode relaxation strengths as obtained from the fit. Finally, in Figure 5 and 6a the comparison between the temperature dependence of the relaxation times and the relaxation strength for *trans*-PI and *cis*-PI is shown.

As expected, it is clear that the relaxation times of both α- and secondary relaxations are independent of the molecular weight in the range studied here. On the contrary, the relaxation time corresponding to the slowest relaxation (normal mode) has systematic molecular weight dependence (see Figure 3). The temperature dependence of the relaxation time corresponding

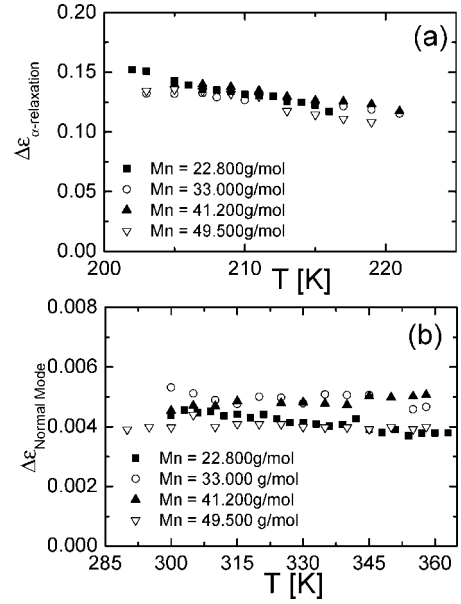

Figure 4. Dielectric relaxation strength, $\Delta\varepsilon$, corresponding to the α-relaxation (a) and normal mode (b) of trans-*PI* at different molecular weights.

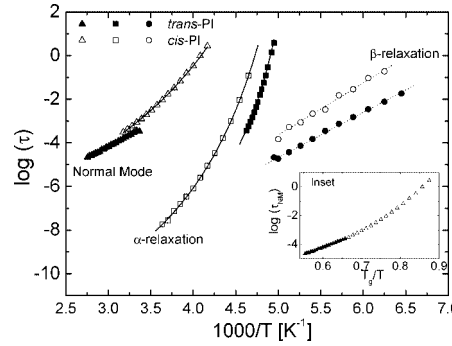

Figure 5. Plot of the characteristic relaxation times of *trans*-PI (filled symbols) and *cis*-PI (open symbols). The solid lines thought the data points are fits of the VFT equation whereas the dotted lines display fits to the Arrhenius equation. Inset: Relaxation times for the normal mode normalized to T_g.

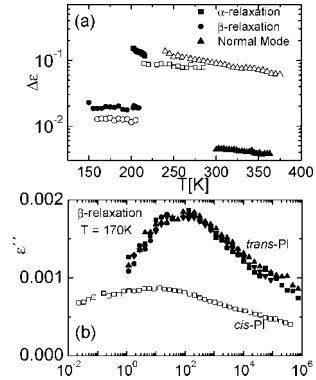

Figure 6. (a) Comparison between the temperature dependence of the dielectric relaxation strength, $\Delta\varepsilon$, corresponding to the normal mode, segmental and secondary relaxations respectively of *trans*-PI (filled symbols) and *cis*-PI (open symbols). (b) Comparison between β-relaxation at 170 K for and *trans*-PI (full symbols) for different molecular weights and *cis*-PI (open symbols).

the α-process, τ_α, is clearly non-Arrhenius and can be well described by the empirical Vogel−Fulcher−Tamman (VFT) equation[38]

$$\tau = \tau_o \exp\left(\frac{DT_o}{T - T_o}\right) \quad (2)$$

where τ_o is the relaxation time extrapolated to infinite temperature and T_o the temperature when it would to diverge. The value of the parameter D is related with the so-called fragility. According to Angell's strong-fragile classification[39] a strong system has an α-relaxation time temperature behavior close to Arrhenius showing a high D-value, whereas a fragile system shows a low D-value in eq 2 and the relaxation times show a more rapid increase close to the glass transition temperature. The results of the VFT fitting are given in Table 2. When discussing fragility it is usual to use the parameter m, instead of D. In terms of the VFT parameters, the fragility index is given by[40]

$$m = \frac{DT_o}{T_{g,100s}\ln(10)}\left(1 - \frac{T_o}{T_{g,100s}}\right)^{-2} \quad (3)$$

where $T_{g,100s}$ is defined as $\tau_\alpha(T_{g,100s}) = 100$ s. Results are shown in Table 2 for both *cis*- and *trans*-PI.

On the other hand, the full width at half-maximum (*fwhm*) of each spectrum was determined from the shape parameters of the HN equation (α and γ) by means of the empirical equation[41]

$$fwhm(\alpha,\gamma) = -0.516 + \frac{1.058}{\alpha} + \frac{0.039}{\gamma} + \frac{0.563}{\alpha\gamma} \quad (4)$$

The so-obtained *fwhm* of α-relaxation is found to be essentially temperature independent in the measured range, *fwhm*(*cis*-PI) = (2.36 ± 0.08) and *fwhm*(*trans*-PI) = (2.54 ± 0.08). The rather low value found for *trans*-PI together with the smooth variation of the relaxation strength with temperature validate that the amorphous phase is not affected by cold crystallization during the measurement time in the temperature range in between 140K to 221K. The *fwhm* values show that the response of *cis*-PI is only slightly narrower compared with *trans*-PI. In addition, we also calculated the *fwhm* corresponding to the component fitting the normal mode for all samples. In this case we obtained *fwhm*(*cis*-PI) = (1.55 ± 0.10) and *fwhm*(*trans*-PI) = (2.32 ± 0.10). This last value was calculated as an average of the samples with different molecular weights. From these values it follows that the response of *trans*-PI is much broader compared with *cis*-PI probably due to the higher polydispersivity of the *trans*-PI as compared with *cis*-PI samples which are almost monodisperse (see Table 1).

Finally, Figure 6b shows a direct comparison between the β-relaxation of *cis*-PI (open symbols) and *trans*-PI (filled symbols) respectively. Clearly, the β-relaxation of *cis*-PI is weaker and broader than that for *trans*-PI. As can be seen in Figure 5, the time scale of both β-relaxations, can be described by Arrhenius equation

Table 2. Fit Parameters for the Segmental Dynamics of All the Samples[a]

Sample	$\log(\tau_o)$ [s]	T_o [K]	D	$T_{g,100}$ [K]	m
trans-PI-22K	−10.5 ± 0.5	177 ± 2	3.6 ± 0.6	199.2	112
trans-PI-33K	−10.5 ± 0.7	179 ± 3	3.4 ± 0.4	200.1	112
trans-PI-41K	−10.5 ± 0.5	179 ± 2	3.3 ± 0.4	199.5	122
trans-PI-49K	−10.5 ± 0.5	179 ± 2	3.4 ± 0.6	200.1	119
cis-PI	−13.4 ± 0.9	165 ± 3	8.7 ± 0.9	205.5	78
trans-PI-22K− CAP phase	−10.0 ± 0.5	194 ± 1	2.5 ± 0.3	211.3	154
trans-PI-33K− CAP phase	−10.0 ± 0.5	193 ± 2	2.3 ± 0.5	209.4	153
trans-PI-49K− CAP phase	−10.0 ± 0.5	193 ± 2	2.3 ± 0.3	209.6	155

[a] The value of $T_{g,100s}$ was calculated as extrapolation to a relaxation time of 100 s. The value of m was calculated from eq 3.

$$\tau(T) = \tau_o \exp\left(\frac{E}{kT}\right) \quad (5)$$

where E represents a mean activation energy, k is Boltzmann's constant and τ_o should correspond to a molecular vibration time. As a result of the fitting, the activation energy was (0.41 ± 0.04) and (0.44 ± 0.04) eV for *trans*-PI and *cis*-PI, respectively, whereas a common value of $\log(\tau_o) = (-14.9 \pm 0.1)$ was obtained for both configurations.

C. Dielectric Relaxation during Isothermal Crystallization of *trans*-PI at 221 K. The isothermal loss spectra (T = 221K) were collected every 2 min during 12 h. During the recording time of each isothermal spectrum, no appreciable change in the dielectric properties was observed. Figure 7a shows the dielectric loss curves at different times for the sample with M_n = 33 kg/mol. Initially (t < 100 s), we can observe a main peak related with the amorphous phase corresponding to the α-relaxation reported above. During crystallization this main loss peak decreases in intensity and shift to lower frequencies. This is the reason why in the following, we will refer to this contribution as α_m-relaxation to distinguish it from the relaxation of the fully amorphous polymer (α-relaxation). Moreover, during crystallization a new process develops at lower frequencies. After 12 h, the overall intensity of the relaxation has strongly decreased and a broad single process dominates the spectrum. The shift of the main loss peak is almost half a decade with respect to the amorphous polymer. The final response is identified with the dynamics of the constrained amorphous phase (CAP) and will be referred to as α_{CAP}. In addition, in the high frequency tail, the β-relaxation contribution is still noted. Very similar results were obtained for the other molecular weights (see Figure 7b) indicating that the overall pattern for the changes in the dielectric spectra during crystallization is independent of molecular weight.

Two different approaches can be used to describe the dielectric response during isothermal crystallization. One is to assume that three relaxation processes are contributing to the dielectric spectra and to fit them with the sum of three arbitrary relaxation functions (a CC to the secondary relaxation, a HN to the segmental relaxation plus another NH to the α_{CAP}

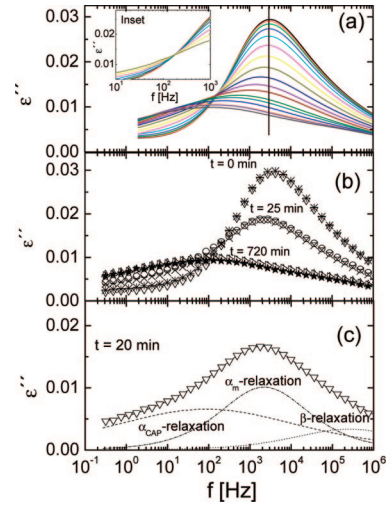

Figure 7. (a) Loss component, ε'', of the complex permittivity, $\varepsilon^*(f)$, during isothermal crystallization at 221 K of *trans*-PI with M_n = 33 kg/mol. Only the curves at: 0, 4, 6, 8, 10, 12, 14, 16, 22, 24, 28, 32, 34, 88, 120, 348, 632 and 720 min are shown. Inset: Loss curves between 0 and 22 min (the isosbestic point is shown). (b) Comparison between isothermal crystallization for samples having different molecular weights. Different symbols represent different molecular weights. (c) Example of the fitting procedure where the α_m, α_{CAP} and β-relaxations are displayed.

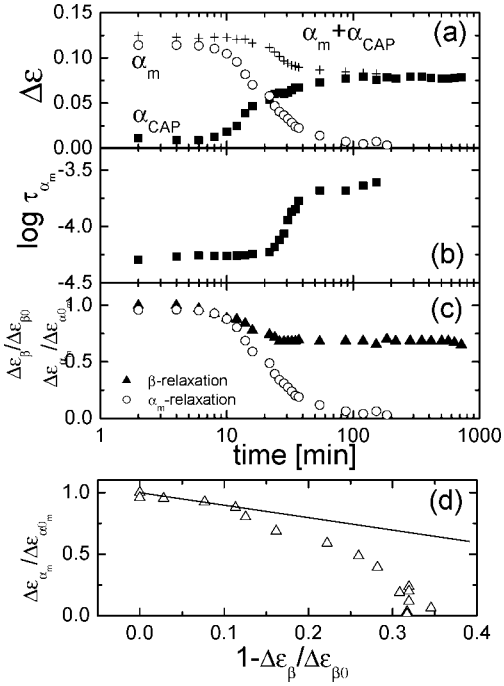

Figure 8. Results of the fitting of the dielectric data for α_m (circles) and α_{CAP} (squares) to the Cole−Cole equations during isothermal crystallization. (a) Dielectric strength ($\Delta\varepsilon$), (b) relaxation times of the α_m process, (c) ratio between the relaxation strength of β- and α_m-relaxations and its initial values ($\Delta\varepsilon_{\beta 0}$ and $\Delta\varepsilon_{\alpha_{m0}}$) and (d) the ratio between $\Delta\varepsilon_{\alpha_m}$ and $\Delta\varepsilon_{\alpha_{m0}}$ versus the ratio between $\Delta\varepsilon_\beta$ and $\Delta\varepsilon_{\beta 0}$.

relaxation). In this case, 11 free parameters are needed to fit the whole dielectric spectra. The second approach is based on the hypothesis that the peak related to the CAP phase keeps both its shape and position during isothermal crystallization. In addition, β-relaxation also keeps its shape and position during crystallization because its local character. Therefore, to fit the time evolution from the complete amorphous to the finally crystallized material, three functions are also necessary (a CC to the secondary relaxation, a CC for the α_{CAP} relaxation and a HN to the α_m-relaxation) but the dynamic parameters associated with both α_{CAP}- and β-relaxations are fixed and obtained from the data after completely crystallization ($t = 12$ h). In this approach, only 6 parameters are necessary to fit the dielectric spectra. Thus, the overall dielectric response can be described by

$$\varepsilon''(\omega,t) = \Delta\varepsilon_{CAP}(t)\varphi_{CAP}(\omega) + \Delta\varepsilon_{\alpha_m}(t)\varphi_{\alpha_m}(\omega,t) + \Delta\varepsilon_\beta(t)\varphi_\beta(\omega) \quad (6)$$

where $\Delta\varepsilon_{CAP}$, $\Delta\varepsilon_{\alpha_m}$, $\Delta\varepsilon_\beta$ are the relaxation strength and $\phi_{CAP}(\omega)$, $\phi_{\alpha_m}(\omega,t)$, $\phi_\beta(\omega)$ are the normalized dielectric loss of the CAP phase, α_m- and β-relaxations respectively. Figure 7c shows an example of this fitting procedure.

The time evolution of the relaxation strength and the relaxation times of the three processes are shown in Figure 8a and Figure 8b respectively whereas in Figure 8c the ratio between $\Delta\varepsilon_\beta/\Delta\varepsilon_{\beta 0}$ and $\Delta\varepsilon_{\alpha_m}/\Delta\varepsilon_{a_{m0}}$ are shown. As seen in Figure 8a, $\Delta\varepsilon_{\alpha_m}$decreases during crystallization and vanish for $t \sim 100$ min whereas the $\Delta\varepsilon_{CAP}$ increases up to the same time and it remains nearly constant during the rest of the experiment. Note that as a result the total intensity ($\Delta\varepsilon_{\alpha_m} + \Delta\varepsilon_{CAP}$) decreases up to $t \sim$ 100min and after that remains essentially constant. As seen in Figure 8b the relaxation time corresponding to the modified segmental dynamics (τ_{α_m}) become about half a decade slower with regards to the fully amorphous material.

Discussion

(a) Dynamics of the Amorphous *trans*-PI−Comparison with *cis*-PI. Now, we focus on the relaxation times and shape of the segmental relaxation of amorphous *trans*-PI as compared with *cis*-PI. First of all, we will analyze the dynamics of *trans*-PI with different molecular weights. As expected, the temperature dependence of the relaxation times corresponding to both α- and β- relaxation does not depend on molecular weight as shown in Figure 3 for the studied molecular weights. Also the relaxation strength corresponding to both α- and β-relaxation has similar values for the different molecular weights (see Figure 4a for α-relaxation). The *fwhm* corresponding to α-relaxation is a very weak function of temperature and, for this reason the time−temperature superposition can be applied to the loss curves of *trans*-PI. The shift of the maximum has been described by using the relationship described by William−Landel−Ferry (WLF)[42]

$$\log(a_T) = \frac{-C_1(T - T_{ref})}{C_2 + (T - T_{ref})} \quad (7)$$

where a_T is the experimentally derived shift factor obtained with a reference temperature, $T_{ref} = 215$ K, close to the glass transition temperature. The WLF-constant C_1 is (8.5 ± 0.3) whereas $C_2 = (41.2 \pm 1.0)$ K for *trans* units. The WLF-constants estimate for *cis* units are $C_1 = (12.5 \pm 0.9)$ and $C_2 = (50.5 \pm 6.0)$ K at $T_{ref} = 215$ K. Note that they are nearly the same as the values reported in the literature.[22] Thus, it follows that the shift factors are different for each configuration, as it could be anticipated by the different values of the fragility index *m*. This difference in the dynamical behavior between *cis* and *trans* units possibly will explain the failure of time temperature superposition on copolymers having different concentration of *cis* and *trans* units.[43]

The relaxation time corresponding to the segmental relaxation in Figure 5 for *trans* units has stronger temperature dependence and faster dynamics than the *cis* units. Moreover, the *m* values shown in Table 2 suggest that PI in *cis* configuration is significantly "stronger" in terms of fragility, than in *trans* configuration. On the other hand, the relaxation strength follows almost the same temperature dependence for both *cis*- and *trans*-units. This could indicate that the perpendicular component of the dipole moment of the *cis*- and *trans*-PI units is both similar, although slightly higher for *trans*-PI. Hatada et al. [44] have reported ^{13}C NMR measurements on both *cis*- and *trans*-PI. In that work it was found that all the carbons in *cis*-PI showed longer T_1 than the *trans*-PI (except for the methyl carbons). This is in qualitatively agreement with the dynamical data shown here where segmental dynamic in *cis*-PI is slower than in *trans*-PI. However, the difference found here in the dynamics of isomers of PI, is different of those for poly(butadiene) (PB), which also can be synthesized in *trans* and *cis* configurations. In spite of the fact that PB has a similar molecular structure than PI, the results recently obtained by means of NMR[45] have shown that the segmental relaxation dynamics of *cis*-PB units exhibit a slightly faster time than the *trans*-PB units, being the opposite to that found here for PI.

The total dipole moment of a monomeric unit (μ) can be decomposed into components perpendicular to ($\mu_\perp$) and parallel to ($\mu_{||}$) the chain contour. As we mentioned above, they are responsible for the segmental and normal mode relaxations respectively. Total electric dipole moments of the monomeric unit in *trans*- and *cis*- configurations can be determined by *ab initio* calculations. The calculations have been performed at the Hartree−Fock (HF) level with a 6-31G(d) basis set and by means of GAMESS code[46] where the main chain carbon atoms of the repeating unit were assigned as C1−C2═C3−C4. Thus, in order to estimate the μ components, we defined the parallel

Table 3. Parallel and Perpendicular Dipole Moment As Estimated by *ab Initio* Calculations[a]

	$\mu_{\parallel}$ [D]	$\mu_{\perp}$ [D]
cis unit	0.132	0.087
trans unit	0.045	0.152

[a] The estimated error is around 10%.

direction as that which links the two outer carbons of the monomeric unit (C1 and C4). This means that the parallel direction depends on configuration (*cis* or *trans*). In Table 3 the results of the calculation of each component of the dipole moment are shown. As expected from the dielectric measurements, the $\mu_{\perp-trans} > \mu_{\perp-cis}$ and $\mu_{\parallel-cis} > \mu_{\parallel-trans}$.

Now, we attempted to determine the ratio of $\mu_{\perp}$ between *cis*- and *trans*-units from the dielectric experiments. On the basis of Onsager−Kirwood equation,[47−49] for a polymer with a perpendicular dipole moment, the relaxation strength can be written as

$$\Delta\varepsilon = \frac{4\pi N\mu^2}{3k_BT}\frac{(\varepsilon_u+2)^2\varepsilon_R}{3(2\varepsilon_R+\varepsilon_U)} \tag{8}$$

where N is the number of monomeric unit in unit volume, μ, is related with the perpendicular component of the effective dipole moment ($\mu^2 = g\,\mu_{\perp}^2$, g being the Kirkwood correlation factor) and $\Delta\varepsilon = \varepsilon_R - \varepsilon_u$. From this expression and assuming a common value for g we can relate $\mu_{\perp}$ in each configuration through the expression

$$\frac{\Delta\varepsilon_{cis}}{\Delta\varepsilon_{trans}} = \frac{\mu_{\perp,cis}^{\ 2}}{\mu_{\perp,trans}^{\ 2}}\frac{(\Delta\varepsilon_{cis}+\varepsilon_U)/(2\Delta\varepsilon_{cis}+3\varepsilon_U)}{(\Delta\varepsilon_{trans}+\varepsilon_U)/(2\Delta\varepsilon_{trans}+3\varepsilon_U)} \tag{9}$$

Taking into account the values of $\Delta\varepsilon$ and $\varepsilon_U = 2.5$ obtained from the dielectric experiments, we obtained $\mu_{\perp,trans} = 1.3\mu_{\perp,cis}$. The ratio obtained from dielectric experiments is slightly lower than that estimated from numerical calculations ($\mu_{\perp,trans} = 1.7\,\mu_{\perp,cis}$). However, we have to note that while *ab initio* calculations were made on a single monomer, the dipole moment based on the data of $\Delta\varepsilon$ is an average of all the monomeric units in the chain. In addition, the same g factor was assumed and likely is not the case.

On the other hand, the normal mode relaxation times depend on molecular weight as this process reflects the global chain motions. For monodisperse *cis*-PI the molecular weight dependence of the relaxation times, scales with M^a where $a \sim 3.5$.[1,3−23] *trans*-PI samples have some polydispersivity (see in Table 1 the polydisperivity index of each sample); thus, since the terminal relaxation is dominated for the longest chains, we chose M_w as the representative molecular weight. Figure 9 shows the result of this analysis. In this way, a value of $a = 3.6 \pm 0.1$ for *trans*-PI is obtained with a temperature dependence similar to that found in *cis*-PI.[1,3−23]

The relaxation time corresponding to the normal mode does not appear to be modified by configuration. In fact, by plotting the relaxation times versus the normalized temperature T_g/T, we can see in inset of Figure 5 that the relaxation times for the normal mode in both configurations are essentially the same. Thus, the local configuration of the chain (*cis*- or *trans*-) seems not to modify the dynamics corresponding to the global chain motions. However, as seen in Figure 6a, the normal mode relaxation strength is more than 1 order of magnitude higher for *cis*-PI. Since the normal mode dielectric relaxation strength of a system having dipoles parallel to the main chain is proportional to the square of the dipole moment along the chain contour[48] it follows that the parallel component of dipole moment associated to *trans*-PI is much smaller than in *cis* configuration. Following a procedure similar to that used above, we have calculated the relation between $\mu_{\parallel}$ for each configuration. In this way, we have obtained $\mu_{\parallel,trans} = 4.2\,\mu_{\parallel},cis$ for the ratio of the parallel component of the dipole moment from dielectric experiments. This ratio is higher than that estimated from numerical calculations (see Table 3).

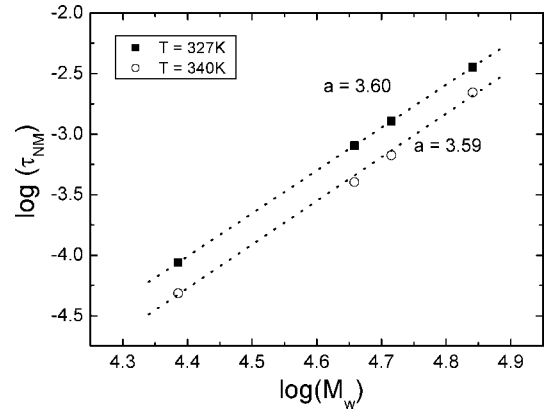

Figure 9. Molecular weight dependence of the maximum relaxation time corresponding to the normal mode of *trans*-PI at two different temperatures. The lines represents the linear fitting.

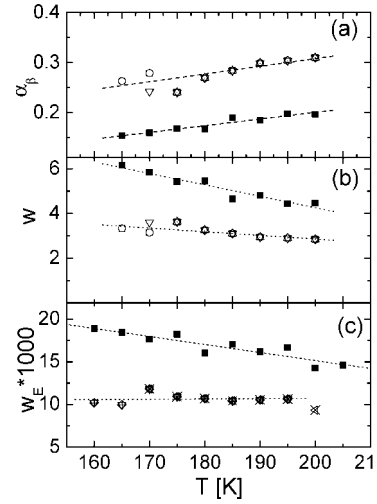

Figure 10. Temperature variation of: (a) the Cole−Cole shape parameter (α_β); (b) the width of log-Gaussian distribution (w); (c) the width of the distribution of energy barriers (w_E) for β-relaxation in *trans*-PI (open symbols) and *cis*-PI (filled symbols).

Finally, the faster β-relaxation, described by the Arrhenius equation, depends on configuration. The value of both pre-exponential factors, τ_o, for *cis* and *trans* units are about 10^{-15}s, which is slightly smaller than the Debye time ($\sim 10^{-14}$ s). In addition, the lower activation energy in the *trans*-PI could indicate a less restricted mobility for this configuration. To our knowledge, the secondary relaxations of *trans*-PI have not been reported in the literature. However, secondary relaxation in *cis*-PI has been studied by Roland et al.[50] by using dielectric spectroscopy and by Pechhold and Blasenbrey[51] by mechanical spectroscopy. The activation energy here estimated for *cis*-PI is about 10% higher that found for *trans*-PI and it is nearly the same as the value of 38.2 kJ/mol previously reported.[50,51]

Now, we will discuss on the shape of the β-process. Usually, the broadening of the secondary relaxations spectra is expected to decrease with increasing temperature (increasing of α_β parameter at higher temperature, see Figure 10a). This is in fact expected by considering a Gaussian distribution of energy barriers as the origin of the extra width with respect to the *fwhm* = 1.14 decades corresponding to a Debye process. In this approach the distribution of the relaxation times results log-Gaussian, being the width (w) given by

$$w = \frac{w_E \log e}{k_B T} \tag{10}$$

where k_B is the Boltzmann constant and w_E represents the width of the Gaussian distribution of energy barriers ($w_E = \sqrt{2}\sigma$ being σ the standard deviation). The width of the distribution of relaxation times (Figure 10b) is larger and more sensible to the temperature in *cis*- than in *trans*- configuration whereas the corresponding width of the distribution of energy barriers (Figure 10c) remains essentially constant for *trans* units in our temperature window but clearly decreases for *cis*-PI. This supports the idea that the environment seen by each monomer in *trans*-PI remains the same in the temperature range considered and the secondary relaxation observed could be associated with a local process. However, the scenario for *cis*-PI is different, since w_E decreases with temperature; the environment seen by the monomer in *cis*-configuration seems to become more homogeneous as temperature increases. In fact, the secondary relaxation in *cis*-PI has been classified as Johari-Golstein (JG) relaxation[50] and this would be in agreement with the temperature dependence here observed for w_E. However, from our results, β-relaxation in *trans*-PI could not be classified as JG.

(b) Dynamics of the Constrained Amorphous Phase (CAP) of *trans*-PI. Now we discuss on the behavior during isothermal cold-crystallization of *trans*-PI which is here reported for the first time. As shown in Figure 7a during 12 h the loss peak related with the amorphous phase vanish completely and a weak and broad slower relaxation emerges. In addition, there is a reduction of the relaxation strength. All this indicates that the polymer fraction that contributes to the dielectric relaxation decreases and changes its dynamics. From the results of the fitting above-described and following the procedure proposed in ref 52, we can estimate the final level of crystallinity by using the ratio between the relaxation strength of β-relaxation after complete crystallization to its initial value: $1 - \Delta\varepsilon_\beta/\Delta\varepsilon_{\beta 0}$ (see Figure 8c). In this way, we got a crystallinity percentage of about (32 ± 3)% for all the molecular weights.

In previous studies about polymer crystallization[53−55] it was possible to define a "crossover frequency" where the loss curves during crystallization cross at a common frequency. This particular frequency was called isosbestic point. This behavior was already observed in the work of Tidy and Williams[53] on poly(ethylene terephtalate) (PET) at short crystallization times but also by Mierzwa and Floudas[54,55] in poly(octadecyl methacrylate) (PODMA) and more recently by Lund et al. [56] in poly(dimethyl siloxane) (PDMS) both for all the primary crystallization time. In the case of the *trans*-PI studied here, we can observe in Figure 7a that an isosbestic point is observed in the earlier stages of crystallization (from 0 to 22 min - see inset of Figure 7a). This is further evidenced by the fact that the peak maximum frequency remains constant during this time range. From Figure 8b it is clear that after this initial period the main relaxation time of the modified amorphous phase (α_m) increases by the presence of *trans*-PI crystals indicating a reduction of the segmental mobility. This is contrary to that previously observd in other flexible polymers such as PDMS[56] or poly(L-lactic acid) (PLLA).[57] However, in more rigid polymers,[52,58−60] the relaxation times were found to be affected by crystallization. Thus, the dielectric characteristics of the dynamics of *trans*-PI during crystallization seem to follow in that aspect the behavior of more rigid polymers. On the other hand, the dielectric relaxation strength of the modified segmental dynamics decrease not only because the increasing of the crystalline phase but also by the presence of the CAP response. By plotting the ratio between $\Delta\varepsilon_{\alpha_m}/\Delta\varepsilon_{a_{m0}}$ versus $1 - \Delta\varepsilon_\beta/\Delta\varepsilon_{\beta 0}$ (measuring the crystallized fraction) we found that this ratio between first decreases linearly up to a crystallization level of about 10% while the CAP response amplitude remains low (see Figure 8d). However, afterward the ratio $\Delta\varepsilon_{\alpha_m}/\Delta\varepsilon_{a_{m0}}$ vanish rather rapidly and the amplitude of the CAP response increases significantly.

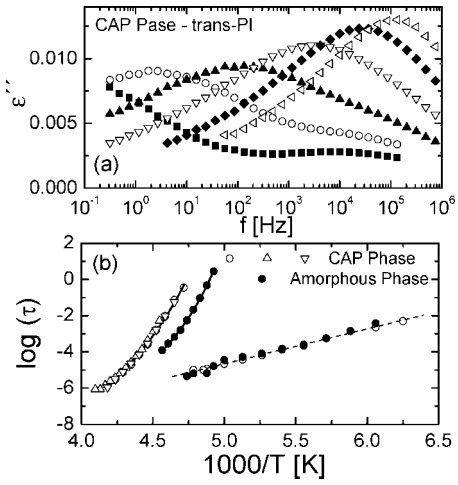

Figure 11. (a) Loss component, ε'', of the complex dielectric permittivity, $\varepsilon^*(f)$ corresponding to the CAP phase at some representative temperatures. (b) Temperature dependence of the relaxation times corresponding to both the CAP (open symbols) and the amorphous phase (filled symbols). Note that, β-relaxation times remain invariant in both phases. Different symbols represent different molecular weights.

Finally, we focus on the temperature evolution of the dielectric loss of a sample crystallized during 12 h at $T = 221$ K where the α_m-relaxation vanishes and the constrained amorphous phase dynamics is evidenced. Figure 11a represents the dielectric loss spectra in this situation, where we observe the α_{CAP}-relaxation plus the β-relaxation on the high frequency side. Both processes are symmetric and were fitted by using CC functions over the temperature range investigated (140−230 K). Note that the dielectric strength corresponding to β-relaxation in both the *CAP* and amorphous phases is essentially independent of temperature, being the averaged values of $\Delta\varepsilon_\beta(CAP) \sim 0.014$ and $\Delta\varepsilon_\beta \sim 0.02$ respectively. Thus, the intensity of β-relaxation obtained by using low temperature data decreases about 30% in the CAP phase, which is in agreement the crystallinity percentage above calculated.

The temperature dependence of the dielectric relaxation time related with both the α_{CAP} and β-relaxations were determined from the fitting procedure and given in Figure 11b. As expected β-relaxation time is insensitive to crystallization. This result is consistent with the behavior reported for other crystalline polymers such as PLLA,[57] poly(propylene succinate) (PPS)[52] or PET.[61] However for poly(ether ether ketone) (PEEK)[62] β-relaxation was founded to be affected by crystallinity.

The temperature dependence of the relaxation time corresponding to α_{CAP} relaxation was fitted by the VFT equation and the parameters are shown in Table 2 for the different molecular weights. Note in Figure 11b that the CAP relaxation times are also independent of molecular weight. The fragility was also calculated by using the parameters in Table 2 and eq. (3). The average fragility for all the molecular weights result in $m_{CAP} = 154$. Thus, the fragility of the CAP phase is larger than in the amorphous phase ($m \sim 118$) which is a situation similar to that observed in PDMS.[56]

Conclusion

In this paper, we have extensively studied, for the first time, the dynamics of *trans*-PI with different molecular weights, in

both the fully amorphous phase and also during and after isothermal crystallization.

We have shown that the local configuration of the chain has a significant effect on the dielectric local and segmental dynamics of PI and this behavior allows explaining the failure of the temperature superposition principle on samples having different concentrations of *cis* and *trans* units. On the contrary the dynamics related to the normal mode have no significant difference between both configurations.

On the other hand, the kinetic during crystallization as observed by dielectric spectroscopy results independent of molecular weight. During crystallization, the dielectric response of *trans*-PI can be fitted by a combination of three processes: the α_m-relaxation related with the modified amorphous phase, the so-called α_{CAP}-relaxation induced by crystallization and the β-relaxation, the two later only varying in relaxation strength. In addition an isosbestic point is observed at earlier times of crystallization. Finally, the dielectric characteristics of the dynamics of *trans*-PI during crystallization seem to follow the behavior of rigid polymers.

Acknowledgment. S.C., A.A and J.C acknowledge the University of the Basque Country and Basque Country Government (UPV 00206.215−13568/2001 and ref. IT-436-07) and Spanish Minister of Education (MAT 2004-01617 and *CSD2006-00053*) for their support. The authors also thank the support of the SoftComp Network of Excelence (NoE) program (NMP3-CT-2004-502235).

References and Notes

(1) Adachi, K.; Kotaka, T. *Macromolecules* **1984**, *17*, 120.
(2) Adachi, K.; Kotaka, T. *Macromolecules* **1985**, *18*, 466.
(3) Adachi, K.; Kotaka, T. *Prog. Polym. Sci.* **1993**, *3*, 585. Adachi, K.; Kotaka, T. *Macromolecules* **1987**, *20*, 2018.
(4) Boese, D.; Kremer, F. *Macromolecules* **1990**, *23*, 829.
(5) Santangelo, P. G.; Roland, C. M. *Macromolecules* **1998**, *31*, 3715.
(6) Abdel-Goad, M.; Pyckhout-Hintzen, W.; Kahle, S.; Allgaier, J.; Richter, D.; Fetters, L. J. *Macromolecules* **2004**, *37*, 8135.
(7) Adolf, D. B.; Ediger, M. D. *Macromolecules* **1991**, *24*, 5834.
(8) Floudas, G.; Reisinger, T. *J. Chem. Phys.* **1999**, *111*, 5201.
(9) Zorn, R.; Arbe, A.; Colmenero, J.; Frick, B.; Richter, D.; Buchenau, U. *Phys. Rev. E* **1995**, *52*, 781.
(10) Arbe, A.; Colmenero, J.; Alvarez, F.; Monkenbusch, M.; Richter, D.; Farago, B.; Frick, B. *Phys. Rev. E* **2003**, *67*, 051802.
(11) Arbe, A.; Colmenero, J.; Alvarez, F.; Monkenbusch, M.; Richter, D.; Farago, B.; Frick, B. *Phys. Rev. Lett.* **2002**, *89*, 245701.
(12) Colmenero, J.; Alvarez, F.; Arbe, A. *Phys. Rev. E* **2002**, *65*, 041804.
(13) Mierzwa, M.; Floudas, G.; Stepanek, P.; Wegner, G. *Phys. Rev. B* **2002**, *62*, 14012.
(14) Haley, J. C.; Lodge, T. P.; He, Y. Y.; Ediger, M. D.; von Meerwall, E. D.; Mijovic, J. *Macromolecules* **2003**, *16*, 6142.
(15) Cangialosi, D.; Alegria, A.; Colmenero, J. *Macromolecules* **2006**, *39*, 7149.
(16) Hoffmann, S.; Willner, L.; Richter, D.; Arbe, A.; Colmenero, J.; Farago, B. *Phys. Rev. Lett.* **2000**, *85*, 322.
(17) Arbe, A.; Alegria, A.; Colmenero, J.; Hoffmann, S.; Willner, L.; Richter, D. *Macromolecules* **2003**, *32*, 7572.
(18) Warneke, S.; Arenskötter, M.; Tenberge, K. B.; Steinbüchel, A. *Microbiology* **2007**, *153*, 347.
(19) Faller, R.; Muller-Plathe, F.; Doxastakis, M.; Theodorou, D. *Macromolecules* **2001**, *34*, 1436.
(20) Faller, R.; Reith, D. *Macromolecules* **2003**, *36*, 5406.
(21) Stockmayer, W. H. *Pure Appl. Chem.* **1967**, *15*, 539.
(22) Watanabe, H. *Macromol. Rapid Commun.* **2001**, *22*, 127.
(23) Watanabe, H. *Prog. Polym. Sci.* **1999**, *24*, 1253.
(24) Anandakumaran, K.; Kuo, C. C.; Mukherji, S. E. *J. Polym. Sci., Part B: Polym. Phys.* **1982**, *20*, 1669.
(25) Kuo, C. C.; Woodward, A. E. *Macromolecules* **1984**, *17*, 1034.
(26) Xu, J. R.; Woodward, A. E. *Macromolecules* **1986**, *19*, 1114.
(27) Davies, C. K. L.; Long, O. E. *J. Mater. Sci.* **1979**, *14*, 2529.
(28) Boochathum, P.; Shimizu, M.; Mita, K.; Tanaka, Y. *Polymer* **1993**, *12*, 2564.
(29) Strobl, G. *Prog. Polym. Sci.* **2006**, *31*, 398.
(30) Allegra, G.; Valdo Meille, S. *Adv. Polym. Sci.* **2005**, *191*, 87.
(31) Ivanov, D. A.; Pop, T.; Yoon, D. Y.; Jonas, A. M. *Macromolecules* **2002**, *15*, 9813.
(32) Zinck, P.; Terrier, M.; Mortreux, A.; Valente, A.; Visseaux, M. *Macromol. Chem. Phys.* **2007**, *208*, 973.
(33) Bonnet, F.; Visseaux, M.; Pereira, A.; Bouyer, F.; Barbier-Baudry, D. *Macromol. Rapid Commun.* **2004**, *25*, 873.
(34) Zinck, P.; Barbier-Baudry, D.; Loupy, A. *Macromol. Rapid Commun.* **2005**, *26*, 46.
(35) Havriliak, S.; Negami, S. *Polymer* **1967**, *8*, 161.
(36) Cole, R. H.; Cole, K. S. *J. Chem. Phys.* **1942**, *10*, 98.
(37) Davidson, D. W.; Cole, R. H. *J. Chem. Phys.* **1951**, *19*, 1484.
(38) (a) Vogel, H. *Phys. Z.* **1921**, *22*, 645. (b) Fulcher, G. S. *J. Am. Chem. Soc.* **1925**, *8*, 339. Fulcher, G. S. *J. Am. Chem. Soc.* **1925**, *8*, 789.
(39) Angell, C. A. *J. Non-Cryst. Solids* **1991**, *131−133*, 13.
(40) Hodge, I. M. *J. Non-Cryst. Solids* **1996**, *202*, 164.
(41) Schwartz, G. A.; Colmenero, J.; Alegría, A. *Macromolecules* **2007**, *40*, 3246.
(42) Ferry J. D. *Viscoelastic properties of polymer*; Wiley: New York , 1980.
(43) Hirose, Y.; Urukawa, O.; Keiichiro, A. J. *Polym. Sci.: Part B: Polym. Phys.* **2004**, *42*, 4084.
(44) Hatada, K.; Kitayama, T.; Terawaki, Y.; Tanaka, Y.; Sato, H. *Polymer Bull.* **1980**, *2*, 791.
(45) He, Y.; Lutz, T. R.; Ediger, M. D. *Macromolecules* **2004**, *37*, 9889.
(46) GAMESS: General Atomic and Molecular Electronic Structure System. Schmidt, M.W.; Baldridge, K. K.; Boatz, J. A.; Elbert, S. T.; Gordon, M. S.; Jensen, J. H.; Koseki, S.; Matsunaga, N.; Nguyen, K. A.; Su, S.; Windus, T. L.; Dupuis, M.; Montgomery, J. A. *J. Comput. Chem.* **1993**, *14*, 1347.
(47) McCrum, N. G.; Read, B. E.; Williams, G. *Anelastic and Dielectric Effects in Polymeric Solids*; Dover Publication: New York, 1991.
(48) Onsager, L. J. *Am. Chem. Soc.* **1936**, *58*, 1486.
(49) Kirkwood, J. G. *J. Chem. Phys.* **1939**, *7*, 911.
(50) Roland, C. M.; Schroeder, M. J.; Fontanella, J. J.; Ngai, K. L. *Macromolecules* **2004**, *37*, 2630.
(51) Pechhold, W.; Blasenbrey, S. *Kautsch. Gummi Kunstst.* **1972**, *25*, 195.
(52) Soccio, M.; Nogales, A.; Lotti, N.; Munari, A.; Ezquerra, T. A. *Phys. Rev. Lett.* **2007**, *98*, 037801.
(53) Williams, G. *Adv. Polym. Sci.* **1979**, *33*, 81.
(54) Mierzwa, M.; Floudas, G. *IEEE Trans. Dielectric EI* **2001**, *8*, 359.
(55) Kremer F.; Schonhals A. *Broadband dielectric spectroscopy*; Springer: Berlin, 2003.
(56) Lund, R.; Alegria, A.; Goitandia, L.; Colmenero, J.; Gonzalez, M. A.; Lindner, P. *Macromolecules* **2008**, *41*, 1364.
(57) Bras, A. R.; Viciosa, M. T.; Wang, Y.; Dionisio, M.; Mano, J. F. *Macromolecules* **2006**, *39*, 6513.
(58) Mijovic, J.; Sy, J. W.; Kwei, T. K. *Macromolecules* **1997**, *30*, 3042.
(59) Alvarez, C.; Sics, I.; Nogales, A.; Denchev, Z.; Funari, S. S.; Ezquerra, T. A. *Polymer* **2004**, *45*, 3953.
(60) Nogales, A.; Ezquerra, T. A.; Denchev, Z.; Sics, I.; Calleja, F. J. B.; Hsiao, B. S. *J. Chem. Phys.* **2001**, *115*, 3804.
(61) Coburn, J. C.; Boyd, R. H. *Macromolecules* **1986**, *19*, 2238.
(62) Kalika, D. S.; Krishnaswamy, R. K. *Macromolecules* **1993**, *26*, 4252.

MA8016585